Smart Mater. Struct., 25(1) p. 015006, 2016.

Prediction of extrinsic charge, voltage, and work-conversion factors for laminated magnetoelectric composites

T.I. Muchenik and E.J. Barbero[1]
West Virginia University, Morgantown USA

Abstract

A magnetoelectric composite produces electricity in response to a magnetic field. The voltage, current, and electric power generated by unit of magnetic field applied to the composite define the intrinsic voltage, current, and power conversion factors. Since the magnetostrictive phase of the composite has a higher magnetic permeability than the surrounding medium, a far field magnetic field is not fully utilized due to demagnetization. Thus, novel explicit equations are developed here to calculate the extrinsic voltage, current, and power conversion factors accounting for demagnetization. The proposed formulation is applied to various materials and geometries to illustrate the process of material and device-geometry selection leading to an optimum design.

Keywords

Piezoelectric, Piezomagnetic, Magnetostrictive, Magnetoelectric, Demagnetization

1 Introduction

Magnetoelectic (ME) devices have potential applications to sensors [1], energy harvesters [2–8], and solid state memory [9]. Although ME materials exist in nature [10], their ME charge coefficient β is too small ($4.13ps\ m^{-1}$ at 2°K [11])[3] and/or their Néel temperature is too low for practical applications, but composite materials can be built to exploit the product property between a strongly *magnetostrictive* (MS) s/H material and a strongly *piezoelectric* (PE) E/s material; that is, obtaining the product ME property E/H, where s, H, E, are the strain, magnetic field, and electric field, respectively.

[1]Corresponding author: ever.barbero@mail.wvu.edu
The final publication is available at http://dx.doi.org/10.1088/0964-1726/25/1/015006
[3]$C\,A^{-1}m^{-1} = s\,m^{-1}$

Unlike naturally occurring ME materials, ME composites can achieve strong ME voltage coefficients. For example, particulate composites can reach 0.16 $V\ A^{-1}$ [12], and laminated composites $\alpha = 5.76V\ A^{-1}$ [4] [13], which corresponds to $\beta \sim 13000ps\,m^{-1}$ at room temperature. While particulate composites are limited in performance by atomic diffusion, mechanical defects, and leakage currents, laminated composites may overcome or minimize these problems [13–15]. Since the ME composite may have other useful properties such stiffness and strength, they may be considered to be *multifunctional* materials as well [16].

While PE materials have an approximately linear strain-electric field response over a wide range of strain or electric fields, MS materials have a nonlinear strain-magnetic field (s-H) response. However, most applications use these materials over a small magnetic-field range centered around a large, fixed magnetic bias. As a result, the behavior may be approximated as linear, and in this later case the material is said to be *piezomagnetic* (PM), and he linear properties used for the PM phase have to be measured at the desired magnetic bias. Variations of all quantities, which should be denoted by a differential or increment (e.g., dH or ΔH) are written simply as H and so on, which from this point forward are understood as the variation of the quantity.

Analytical models [17–21] are useful because they can be used to quickly predict approximate values for the expected voltage, charge, or work conversion of the device as a function of material properties for the PE and PM materials as well as a function of the relative volume fractions of the constituents. An analytical model to predict the *intrinsic* ME response of laminate composites is presented in [21] for all four possible laminate configurations (TT, LT, TL, and LL), correctly taking into account the conductivity of the PM phase. However, intrinsic response is not representative of *device* performance because the far field magnetic field is not fully utilized due to demagnetization, which is caused by the magnetostrictive phase of the composite having a higher magnetic permeability than the surrounding medium. Thus, novel explicit equations are developed herein to calculate the *extrinsic* voltage, current, and power conversion factors accounting for demagnetization, which unlike for intrinsic properties, requires to account for the geometry of the device[5].

The ME voltage coefficient provides a indication of the ME material's performance to produce an electric field E, and thus voltage $V = E\ t$ from exposure to a magnetic field H, when no work is drawn from the device[6]. Similarly, the ME charge coefficient represents the performance of the ME material to produce an electric displacement D, and thus charge $Q = DA$ from exposure to a magnetic field H, again when no work is drawn from the device[7]. Finally, the ME coupling factor κ yields a measure of the ME material's performance to convert magnetic work into electric work [21–23].

The formulas for these coefficients require calculation of the dielectric permittivity of the

[4] $V\ A^{-1} = 796mV cm^{-1} Oe^{-1}$

[5] In this work, the composite is called a "material" as long as the geometrical dimensions of the "device" are not relevant. The dimensions are relevant due to demagnetization, requiring the use of the term "device" to emphasize the dependency of the device behavior with geometrical dimensions. Volume fractions are not dimensions. The PM and PE are called "phases" to emphasize that they are not composites and do not have intrinsic ME effect.

[6] Where t is the total thickness of the device, E is the average electric field over t, and V is the voltage measured across the thickness t of the device.

[7] Where A is the area of the device.

Property	BTO	PZT-2	PZT-4	PZT-5A	PZT-5H	PZT-8	PVDF	Units
S_{11}	8.6	11.6	12.3	16.4	16.5	11.5	365	$10^{-12}m^2N^{-1}$
S_{33}	9.1	14.8	15.5	18.8	20.7	13.5	472	$10^{-12}m^2N^{-1}$
S_{12}	-2.6	-3.33	-4.05	-5.74	-4.78	-3.7	-209	$10^{-12}m^2N^{-1}$
S_{23}	-2.7	-4.97	-5.31	-7.22	-8.45	-4.8	-192	$10^{-12}m^2N^{-1}$
ϵ_{33}/ϵ_0	1200	450	1300	1700	3400	1000	13	
μ_{11}/μ_0	1	1	1	1	1	1	1	
μ_{33}/μ_0	1	1	1	1	1	1	1	
d_{31}	-58	-60.2	-123	-171	-274	-37	21	$10^{-12}CN^{-1}$
d_{33}	149	152	289	374	593	225	-26	$10^{-12}CN^{-1}$

Table 1: PE material properties [24–26]. The compliance is measured at constant electric field and the dielectric constant is measured at constant stress.

device ϵ^H at constant magnetic field and magnetic permeability of the device μ^E at constant electric field, but the well known series/parallel capacitor formulas are not appropriate for PM devices because the application of a magnetic field results in an electrical displacement and vice versa, due to the inherent coupling present in the device. Thus, the methodology proposed in [21] is used here to derive close form, explicit formulas for their calculation.

The demagnetizing effect has been considered by other researchers, allowing them to obtain extrinsic properties for particular geometries and configurations. In this work, explicit equations are obtained for all four possible configurations (TT,TL,LT,LL) by using the averaged demagnetizing factor approximation. Twenty-eight combinations of seven PM and four PE materials are studied to elucidate the effects of material properties, volume fraction, and device geometry on voltage, charge, and work-conversion. ME properties are calculated to find the optimum PM/PE materials combinations and PM volume fraction χ for the four configurations (TT, TL, LT, LL). Optimum values are computed for 3 measures of performance, namely ME voltage coefficient α, ME charge coefficient β, and ME coupling factor κ. Thorough explanations are presented for the trends observed.

2 Materials and constitutive equations

The PE and PM materials selected for this study are listed in Tables 1 and 2, respectively. Some properties not available for Galfenol and Metglas are calculated using the same ratios S_{11}/S_{33}, ν_{12}/ν_{31} and q_{31}/q_{33} of Terfenol-D. The mechanical properties of CFO [8] are assumed to be isotropic. The DC magnetic bias used to measure the properties of the PM phase is indicated in Table 2. A low magnetic bias is desired for most applications, so that a smaller permanent magnet can be used. This gives a design advantage to Metglas and Galfenol.

The analytical model from [21] is summarized first. It starts with the multi-physics

[8] CFO stands for $CoFe_2O_4$

Property	Terfenol-D	Galfenol	Metglas	CFO	Units
S_{11}	44	20.3	52.7	6.5	$10^{-12}m^2N^{-1}$
S_{33}	38	17.5	45.5	6.5	$10^{-12}m^2N^{-1}$
S_{12}	-11	-5.1	-13.2	-2.37	$10^{-12}m^2N^{-1}$
S_{23}	-16.5	-7.6	-19.7	-2.37	$10^{-12}m^2N^{-1}$
ϵ/ϵ_0	∞	∞	∞	∞	
μ_{33}/μ_0	3	260	17000	2	
q_{31}	-4300	-23271	-460353	556	$10^{-12}mA^{-1}$
q_{33}	8500	46000	910000	-1880	$10^{-12}mA^{-1}$

Table 2: PM material properties [19, 25, 27], CFO stands for $CoFe_2O_4$. The compliance is measured at constant magnetic field and the magnetic permeability is measured at constant stress.

constitutive equations

$$s = S\sigma + d^T E + q^T H \quad (1)$$
$$D = d\sigma + \epsilon E \quad (2)$$
$$B = q\sigma + \mu H \quad (3)$$

where σ is the stress tensor, s is the strain tensor, E is the electric field vector, H is the magnetic field vector, D is the electric displacement vector, B is the magnetic flux density vector, S is the compliance tensor (measured at constant electric and magnetic field), ϵ is the dielectric permittivity tensor (measured at constant stress), μ is the magnetic permeability tensor (measured at constant stress), d is the PE charge constant tensor, and q is the PM constant tensor. These equations describe the behavior of the PM and PE phases. PM materials are actually magnetostrictive, with a nonlinear relationship between strain and magnetic field, but they are customarily treated as linear in the close neighborhood of an applied *magnetic bias*. Then, the PM constant tensor and all the PM properties are measured at this magnetic bias.

PE and PM materials display transverse isotropy on a plane normal to the *polarization (magnetization)* direction, which is denoted by the 3-axis in this work. By design, the material's 3-axis is placed along the expected direction for E and H fields in order to obtain maximum performance. The polarization and magnetization directions do not coincide for the TL and LT configurations. Therefore, a global coordinate system (Figure 1) is used to cast the equations after appropriate coordinate transformation for each of the phases.

The compliance tensor S is defined as follows [28, (1.91)]

$$S = \begin{bmatrix} S_{11} & S_{12} & S_{23} & 0 & 0 & 0 \\ S_{12} & S_{11} & S_{23} & 0 & 0 & 0 \\ S_{23} & S_{23} & S_{33} & 0 & 0 & 0 \\ 0 & 0 & 0 & S_{44} & 0 & 0 \\ 0 & 0 & 0 & 0 & S_{44} & 0 \\ 0 & 0 & 0 & 0 & 0 & 2(S_{11}-S_{12}) \end{bmatrix} \quad (4)$$

The PE charge constant tensor d is defined as

$$d = \begin{bmatrix} 0 & 0 & 0 & 0 & d_{15} & 0 \\ 0 & 0 & 0 & d_{15} & 0 & 0 \\ d_{31} & d_{31} & d_{33} & 0 & 0 & 0 \end{bmatrix} \tag{5}$$

where

$$d_{ij} = \frac{s_j}{E_i}\Big]_{\sigma=0} = \frac{D_i}{\sigma_j}\Big]_{E=0} \tag{6}$$

The PM constant tensor q is defined in the same way, where

$$q_{ij} = \frac{s_j}{H_i}\Big]_{\sigma=0} = \frac{B_i}{\sigma_j}\Big]_{H=0} \tag{7}$$

The dielectric permittivity ϵ, and magnetic permeability μ, are diagonal tensors defined as

$$\epsilon = \epsilon_{ij}\delta_{ij} \tag{8}$$

$$\mu = \mu_{ij}\delta_{ij} \tag{9}$$

where δ_{ij} is the Kronecker symbol and x_3 is the axis of transverse isotropy, which coincides with the direction of polarization or magnetization ($\epsilon_{11} = \epsilon_{22}$ and $\mu_{11} = \mu_{22}$).

ME devices can be built using four different configurations (Figure 1): transverse magnetization with transverse polarization (TT), longitudinal magnetization with transverse polarization (LT), transverse magnetization with longitudinal polarization (TL), and longitudinal magnetization with longitudinal polarization (LL), as shown in Figure 1. Intrinsic voltage, charge, and coupling factors are found by applying boundary conditions representing each case [21, § 2.1–2.4].

For simplicity, only two layers are shown in Figure 1, but it is assumed that the actual device is symmetrically laminated. Furthermore, the laminas are thin in comparison to the in-plane dimensions, resulting in a state of plane stress [28] and insignificant shear lag effect [29]. As a result, the stresses are averaged through the thickness of each lamina and the intralaminar/interlaminar shear strains are negligible [28]. Consequently, the ME pair is assumed to be fully effective over its entire area.

The PE phase is most commonly polarized in the transverse direction. Otherwise, an insulator is needed at the interface to prevent charge leakage from the PE through the PM phase, since the latter is highly conductive. For example, a longitudinally polarized PZT was bonded to two magnetostrictive FeBSiC alloy (Metglas) foils, using two Kapton films in between to confine the electric field to the PE phase, thus avoiding leakage [30].

3 Intrinsic properties

Intrinsic properties are calculated first for the 28 material combinations to establish a baseline for subsequent comparison with the extrinsic properties. This is necessary because extrinsic properties also depend on geometry but intrinsic do not. In this way, it is possible to better elucidate the material effects separately from the geometrical and the demagnetization effects. Intrinsic properties are calculated with the equations presented in [21].

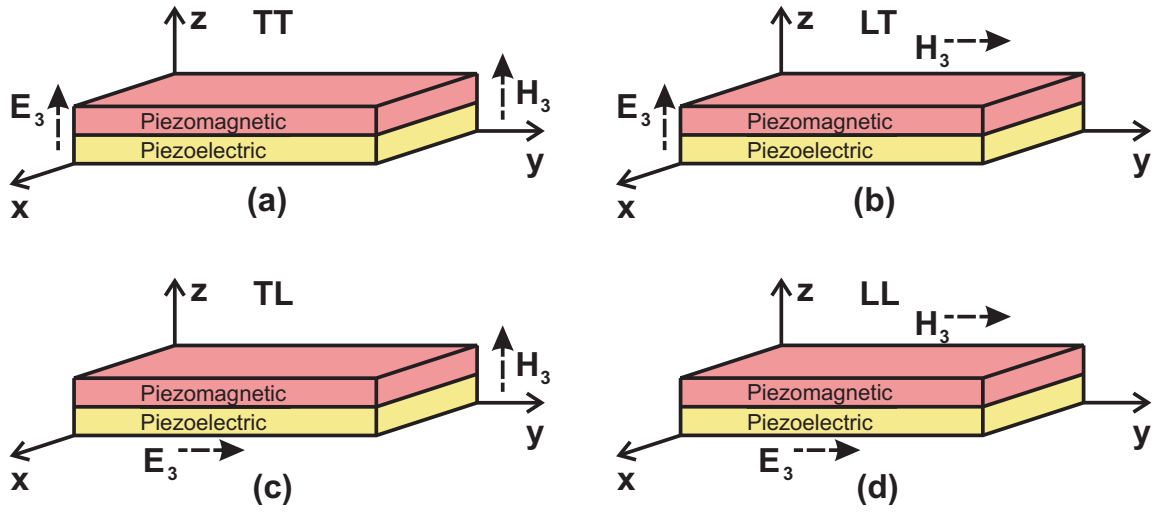

Figure 1: Laminate configurations: (a) transverse magnetization and transverse polarization (TT), (b) Longitudinal magnetization and transverse polarization (LT), (c) transverse magnetization and longitudinal polarization (TL), and (d) longitudinal magnetization with longitudinal polarization (LL). Reproduced from [21] with permission.

3.1 TT configuration

3.1.1 ME coupling factor

Power output from the ME composite requires a high ME coupling factor κ, formally defined as the ratio of electric work harvested to magnetic work applied [21, Eq. (50)]. The intrinsic ME coupling factor κ of the TT configuration is calculated for the 28 material combinations. The results are shown in Figure 2. The highest coupling factor ($\kappa = 0.17$) is obtained for Terfenol-D/PZT-5H composite with PM volume fraction $\chi = 85\%$.

Composites with Terfenol-D and other PZT compositions result in slightly lower ME coupling factors with similar volume fraction dependency. The highest values are obtained for the compositions with higher PE coupling factor. Terfenol-D/BTO has a similar dependency on the PM volume fraction as Terfenol-D/PZT but with smaller values of κ due to the smaller PE coupling factor of BTO. Finally, Terfenol-D/PVDF has the smallest ME coupling factor due to the smallest PE coupling factor of PVDF.

For Terfenol-D/PVDF, it can be observed that the optimum ME coupling is obtained for smaller PM volume fraction χ compared to Terfenol-D/PZT-5H. This is due to the higher compliance of PVDF, which requires a smaller amount of PM phase to obtain the optimum strain.

Regarding the influence of the PM phase, the highest ME coupling is obtained for Terfenol-D, even though it does not have the highest PM coupling factor. Although Metglas has the highest PM coupling factor, it does not yield the highest ME coupling factor because of its high magnetic permeability. A high magnetic permeability affects the distribution of H between PM and PE phases which detrimentally affects performance.

The distribution of H between PM and PE phases is obtained from (3). The magnetic

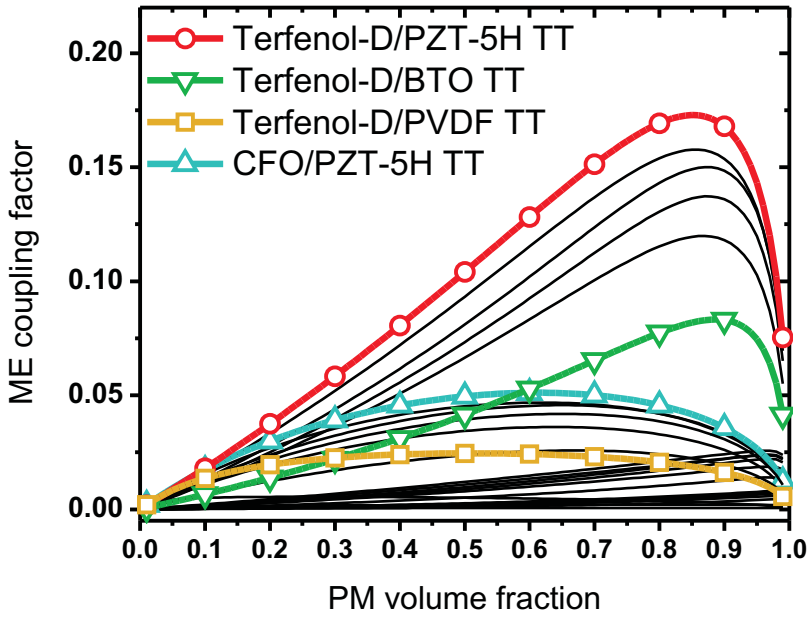

Figure 2: Intrinsic ME coupling factor in TT configuration, (dimensionless) for all material combinations. Metglas based composites not labeled because they display very low coupling in this situation (see text).

flux density in the z-direction for the PM phase is

$$B_z^{PM} = 2q_{31}^{PM}\sigma_x^{PM} + \mu_{33}^{PM}H_z^{PM} \tag{10}$$

and the magnetic flux density for the PE phase is

$$B_z^{PE} = \mu_{33}^{PE}H_z^{PE} \tag{11}$$

When transverse magnetization is used, the magnetic flux density B in both phases are equal $B_z^{PE} = B_z^{PM}$. Combining equations (10) and (11) we get

$$\mu_{33}^{PE}H_z^{PE} = 2q_{31}^{PM}\sigma_x^{PM} + \mu_{33}^{PM}H_z^{PM} \tag{12}$$

In (12), if the PM phase has a magnetic permeability μ_{33}^{PM} much higher than the PE phase μ_{33}^{PE}, a smaller magnetic field H_z^{PM} in the PM phase is observed. This smaller magnetic field reduces the magnetic work harvested by the PM phase. Therefore, for transverse magnetization, a smaller magnetic permeability increases the magnetic field (and the magnetic work harvested) in the PM phase. After Terfenol-D, CFO shows the next higher ME coupling factor, for the same reason.

The effect of the high magnetic permeability on the effective internal magnetic field is further discussed in Section 4 to account for demagnetization.

The optimum PM volume fraction with CFO is smaller than with Terfenol-D because CFO, having smaller compliance, generates more stress to drive the PE phase with less PM volume fraction χ than Terfenol-D.

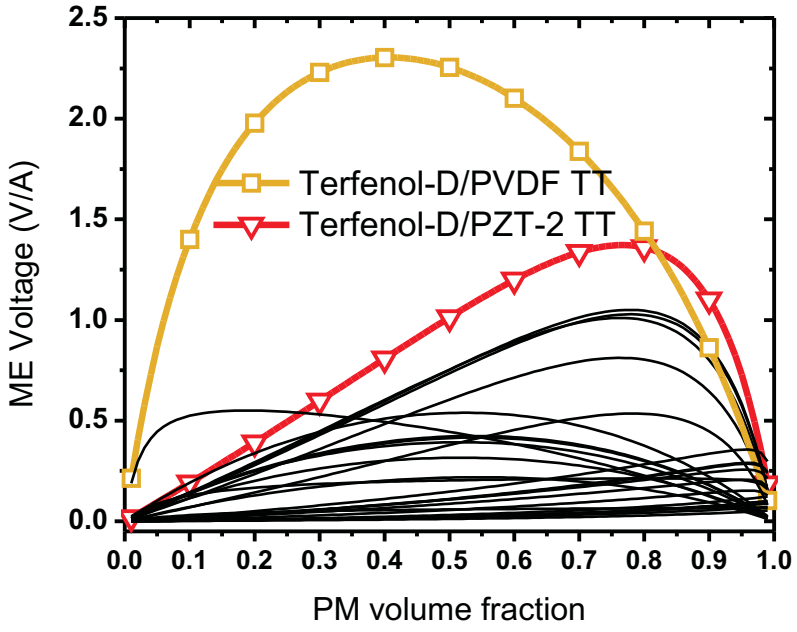

Figure 3: Intrinsic ME voltage coefficient (TT configuration) for all material combinations.

3.1.2 ME voltage coefficient

To obtain high open circuit sensitivity requires high ME voltage coefficient α [21, Eq. (23)]. The ME voltage coefficient for the 28 different material combinations in the TT configuration are shown in Figure 3. The highest ME voltage ($2.3VA^{-1}$) is obtained with Terfenol-D/PVDF composite with a PM volume fraction χ =41% ($\kappa = 0.024$).

Another configuration with a high ME voltage coefficient ($1.4VA^{-1}$) is Terfenol-D/PZT-2 composite with PM volume fraction 77%. The optimum α is obtained for higher PM volume fractions because of the higher stiffness of PZT-2, requiring more PM phase to achieve the optimum strain.

3.1.3 ME charge coefficient

To obtain a high short circuit sensitivity, a high ME charge coefficient β is required [21, Eq. (25)]. The ME charge coefficient for the selected composites in the TT configuration are shown in Figure 4. In this case, the highest β is obtained when $\chi \to 1$, because the effective area to produce the electric displacement D does not change with the PM volume fraction. Then, $\chi \to 1$ maximizes the stiffness of the PM phase [21] and thus maximizes the strain transferred to the PE phase. However, $\chi \to 1$ results in a ME coupling factor $\kappa = 0$, making impossible the measurement. Therefore, a compromise between β and κ is required. The criterion used in this work to achieve this compromise consist in selecting a PM volume fraction that has a high β while retaining 70% of the maximum κ for that configuration. In the case of Terfenol-D/PZT-5H, 70% of the maximum κ is 0.12, which can

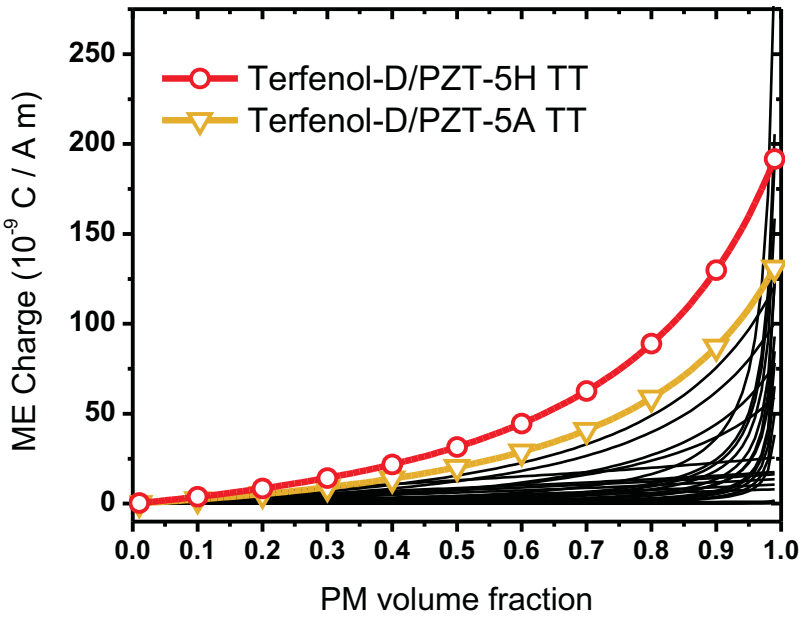

Figure 4: Intrinsic ME charge coefficient (TT configuration) for all material combinations.

be obtained with $\chi = 97\%$, resulting in $\beta = 175 \times 10^{-9} C\, A^{-1} m^{-1}$. Furthermore, composites using PZT-5H posses a high ME charge coefficient due to the high PE charge coefficient ($d_{31} = 274 \times 10^{-12} C N^{-1}$) of PZT-5H (Table 1).

3.2 LT configuration

Here the PM is magnetized in the longitudinal direction, i.e., along the longest dimension of the laminate. Longitudinal magnetization results in an increase of the magnetic field in the PM phase compared to transverse magnetization, because (unlike for the TT configuration) the magnetic field is applied at the edges of the PM phase without having to cross the PE phase ($H^{PM} = H^{PE} = H_3$). This is an advantage for the materials with high magnetic permeability μ_{33}^{PM} such as Metglas. This effect will be further discussed when the extrinsic properties are calculated accounting for the demagnetizing effect in Section 4. Additionally, the PM coupling coefficient κ_{33} is higher in the direction of magnetization than κ_{31} for the TT configuration.

3.2.1 ME coupling factor

The increase of the magnetic field in the PM phase results in a higher magnetic work harvested (compared with transverse magnetization). This can be observed in Figure 5 were the ME coupling coefficient of composites (LT configuration) using Metglas show better performance that anything in Figure 2.

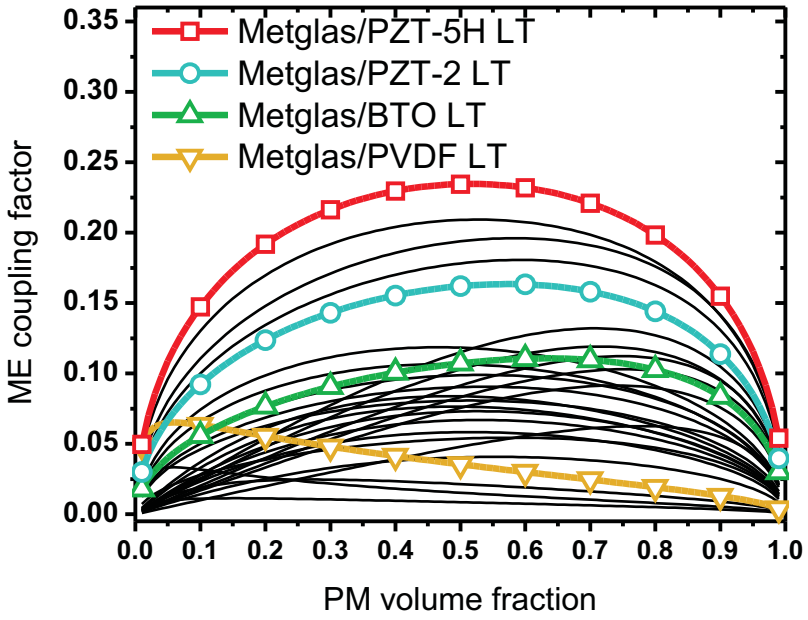

Figure 5: Intrinsic ME coupling factor (dimensionless) in LT configuration for all material combinations.

Regarding the PE phase, the same materials used for the TT configuration give the optimum response. Metglas/PZT-5H composite (LT configuration) with a PM volume fraction of 53% has a ME coupling factor of 0.23 and Metglas/BTO composite with a PM volume fraction of 64% has a ME coupling factor of 0.11.

3.2.2 ME voltage coefficient

The improvement obtained by magnetization in the longitudinal direction is observed in the ME voltage coefficient as well (Figure 6). Here it can be seen that Metglas/PVDF composite has the highest $\alpha = 274 V A^{-1}$ with a PM volume fraction of 29% ($\kappa = 0.05$). Another composite of interest is Metglas/PZT-2, which has smaller ME voltage coefficient ($119 V A^{-1}$) but higher ME coupling factor ($\kappa = 0.16$) for a PM volume fraction of 66%.

3.2.3 ME charge coefficient

The highest values of ME charge coefficient are obtained for the LT configuration due to the high strain produced by the PM phase and the large effective area of the PE phase. Predictions are shown in Figure 7.

If the criterion discussed in Section 3.1.3 is used for the Metglas/PZT-5H composite in the LT configuration, the PM volume fraction to achieve 70 % of the optimum ME coupling is 89%, resulting in a good compromise between ME charge coefficient ($\beta = 8393 \times 10^{-9} C\, A^{-1} m^{-1}$ and coupling factor $\kappa = 0.16$). An alternative for a lead free material is

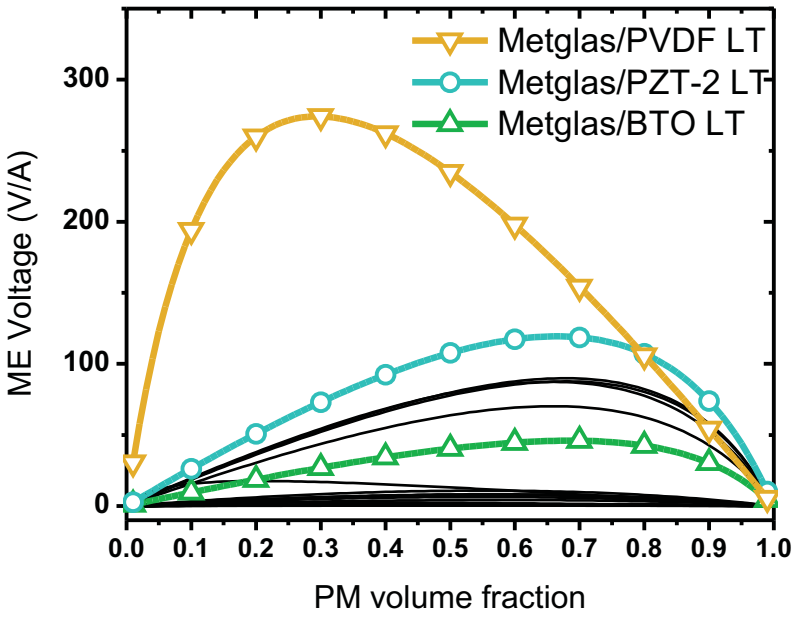

Figure 6: Intrinsic ME voltage coefficient for all the material combinations for the LT configuration.

Metglas/BTO composite with a PM volume fraction of 92%, which results in $\beta = 3219 \times 10^{-9} C\, A^{-1} m^{-1}$ and $\kappa = 0.08$.

3.3 TL configuration

Here the composite is magnetized in the transverse direction but charge/voltage are sensed at the ends of the longitudinal direction. Polarization of the PE phase in the longitudinal direction is more challenging requiring and insulator at the PM/PE interface, but ME coupling factor and voltage coefficient are increased. The use of the TL configuration results in smaller ME coefficients and coupling compared to LL and LT configurations. This is due to the smaller magnetic field in the PM phase, as it was discussed in Section 3.1.1. For this reason, this configuration will not be discussed further, but predictions can be obtained using the formulas provided in the Website [31].

3.4 LL configuration

The highest α and κ is predicted when the ME composite is polarized and magnetized in the longitudinal direction, justifying the more complicated fabrication required by longitudinal polarization, including an insulator.

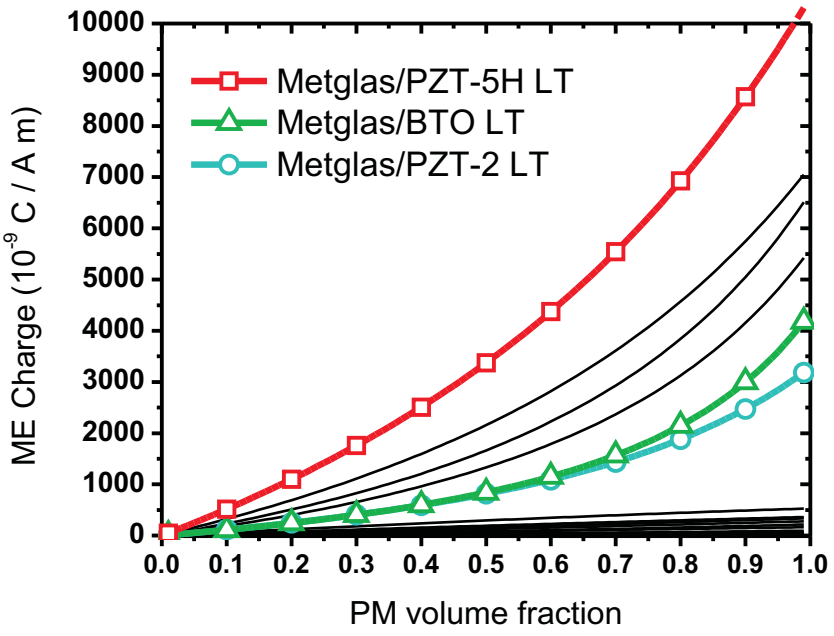

Figure 7: Intrinsic ME charge coefficient (LT configuration) for all material combinations.

3.4.1 ME coupling factor

Predicted ME coupling factors for LL configuration are shown in Figure 8. Metglas/PZT-5H has the highest ME coupling factor (0.56) at 57 % PM volume fraction. This is due to the high PM and PE coupling factors of Metglas and PZT-5H, respectively. For this configuration the coupling factor k_{33} and k_{31} are important because strain is produced in the x- and y-directions. For a lead free material Metglas/BTO with a PM volume fraction of 69% ($\kappa = 0.33$) is the best option.

3.4.2 ME charge coefficient

Predictions for the ME charge coefficient can be seen in Figure 9. Metglas/PZT-5H composite has a ME charge coefficient of $4246 \times 10^{-9} C\, A^{-1} m^{-1}$ and $\kappa = 0.56$ for a PM volume fraction of 60%. The β is smaller than the value for the LT configuration but the coupling coefficient associated is three times higher. Metglas/BTO composite is a good alternative to PZT, yielding $\beta = 1423 \times 10^{-9} C\, A^{-1} m^{-1}$ and $\kappa = 0.33$ for a PM volume fraction of 69%.

3.4.3 ME voltage coefficient

The ME voltage coefficient for the LL configuration can be seen in Figure 10. Metglas/PZT-2 composite reaches a good compromise (according to the established criterion) between the ME voltage coefficient and the ME coupling factor at PM volume fraction of 92%, resulting in $\alpha = 2705 V A^{-1}$ and $\kappa = 0.32$.

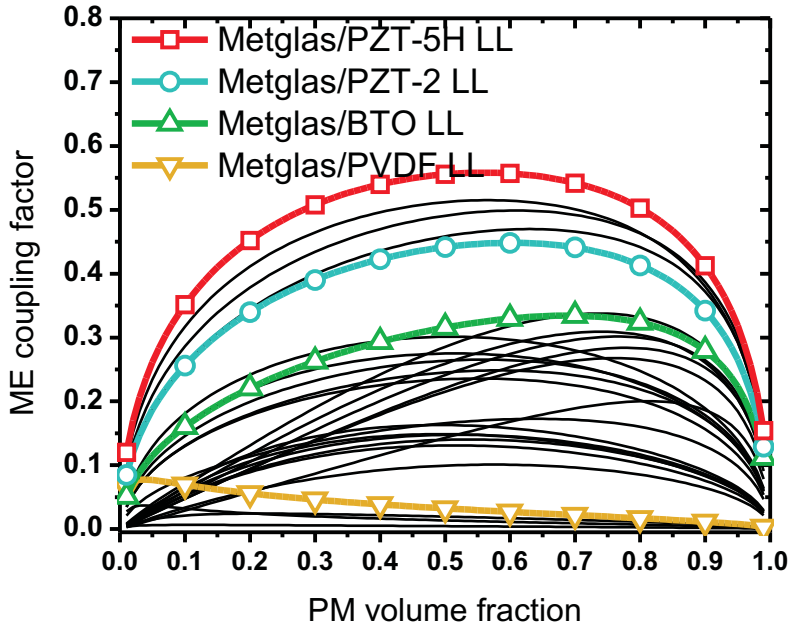

Figure 8: Intrinsic ME coupling factor (dimensionless) in LL configuration for all material combinations.

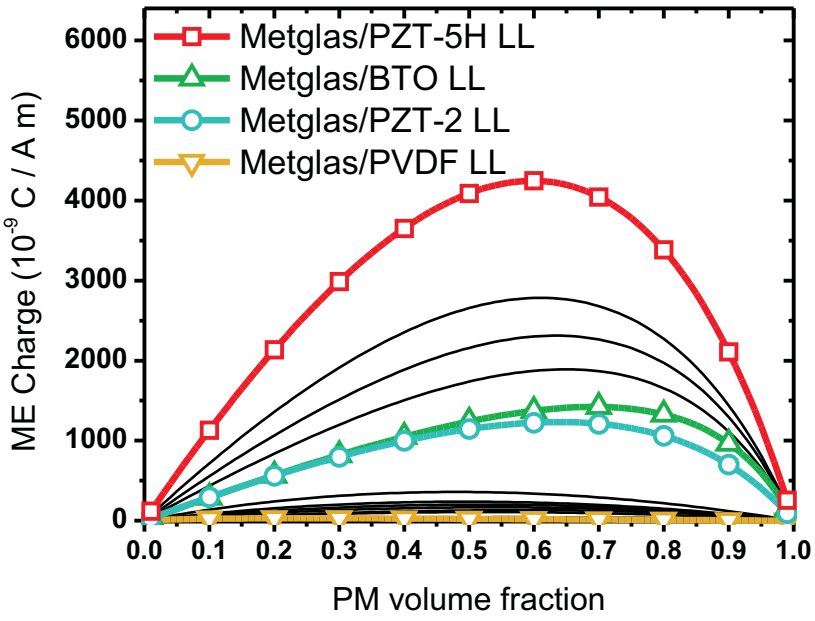

Figure 9: Intrinsic ME charge coefficient (LL configuration) for all material combinations.

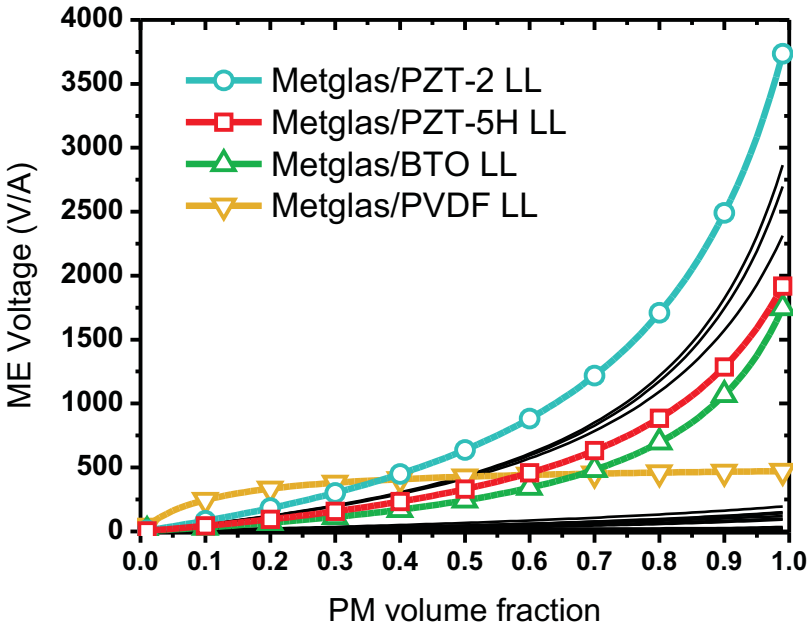

Figure 10: Intrinsic ME voltage coefficient for all the material combinations for the LL configuration.

Metglas/PVDF composite shows an unusual behavior as a function of the PM volume fraction. For $\chi < 0.4$, increasing the PM volume fraction increases the ME voltage coefficient, but after 40% the ME voltage coefficient remains practically constant. This is due to the fact that the elastic modulus of PVDF is more than six times smaller than the elastic modulus of Metglas. As a result, only a small volume fraction of Metglas is required to produce high strain in the PVDF layer and higher volume fractions of Metglas practically do not increase the strain in the PVDF.

A similar effect can be seen in the ME coupling factor (Figure 8). The compromise between the ME voltage coefficient and coupling factor for Metglas/PVDF in LL configuration is obtained for PM volume fraction of 22%, resulting in $\alpha = 345VA^{-1}$ and $\kappa = 0.05$. Another lead free option is Metglas/BTO composite with a PM volume fraction of 94% having a ME voltage of $1304VA^{-1}$ and a coupling factor of 0.24.

3.5 Summary of intrinsic properties

Composites with high open circuit sensitivity are shown in Table 3. Longitudinal magnetization yields higher coefficients due to the higher strain produced and Metglas is the best PM phase for this configuration. The first three composites require the more complex longitudinal polarization but produce higher ME voltage coefficient (α). For the first three composites, a PM volume fraction lower than the optimum ($\chi \to 1$) is selected to avoid $\kappa = 0$. The highest performance PE phase is PZT-2. For lead free composites, BTO followed by PVDF provide the best performances. High open circuit sensitivity is the only

PM Phase	Metglas	Metglas	Metglas	Metglas	Metglas	Metglas	n/a
PE Phase	PZT-2	PVDF	BTO	PVDF	PZT-2	BTO	n/a
Configuration	LL	LL	LL	LT	LT	LT	n/a
χ	92%[a]	22%[a]	94%[a]	29%	66%	69%	
α	2705	345	1304	274	119	46	V/A
κ	0.32	0.05	0.24	0.05	0.16	0.11	
β	595	31	686	43	1290	1522	$10^{-9}C/(A\,m)$

Table 3: ME composites with high intrinsic voltage coefficient for open circuit sensors application. [a]The optimum PM volume fraction ($\chi \to 1$) is not used to avoid $\kappa = 0$, but PM volume fraction is selected to retain 70% of the maximum ME coupling factor for each configuration.

PM Phase	Metglas	Metglas	Metglas	Metglas	n/a
PE Phase	PZT-5H	BTO	PZT-5H	BTO	n/a
Configuration	LT	LT	LL	LL	n/a
χ	89%[a]	92%[a]	60%	69%	
β	8393	3219	4246	1423	$10^{-9}C/(A\,m)$
κ	0.16	0.08	0.56	0.33	
α	45	26	458	465	V/A

Table 4: ME composites with high intrinsic charge coefficient for closed circuit sensor applications. [a]The optimum PM volume fraction ($\chi \to 1$) is not used to avoid $\kappa = 0$, but PM volume fraction is selected to retain 70% of the maximum ME coupling factor for each configuration.

application where PVDF shows good performance because its small PE charge coefficient and coupling factor results in small β and κ.

Composites with high closed circuit sensitivity are shown in Table 4. Transverse polarization results in a higher closed circuit sensitivity due to the higher area at which the electric displacement is produced. PZT-5H results in the highest β between the PE materials selected due to its high PE charge coefficient (d). Smaller PM volume fraction than the optimum ($\chi \to 1$) is selected to achieve a good trade off between κ and β for the LL configuration.

Composites with longitudinal polarization have about half the ME charge coefficient compared with transverse polarization. For the PM phase, Metglas in longitudinal magnetization has the highest performance. Lead free ME composites for closed circuit applications can be fabricated using BTO with the disadvantage of decreasing β to about a third.

Composites with high ME coupling factor are shown in Table 5. ME harvesters require that most of the harvested magnetic work is transformed to electric work, requiring a structure with high ME coupling factor (κ). Among the materials considered in this study, the composite that better satisfies this is Metglas/PZT-5H in LL configuration with a PM volume fraction of 60%, which results in $\kappa = 0.56$ (Table 5).

Composites with transverse polarization have κ more than two times smaller due to the smaller k_{31} of the PE phase. Using lead free BTO in the LL configuration reduces the ME

PM Phase	Metglas	Metglas	Metglas	Metglas	n/a
PE Phase	PZT-5H	BTO	PZT-5H	BTO	n/a
Configuration	LL	LL	LT	LT	n/a
χ	60%	69%	53%	64%	
κ	0.56	0.33	0.23	0.11	
α	458	465	66	46	V/A
β	4246	1423	3657	1305	$10^{-9}C/(A\,m)$

Table 5: ME composites properties with high intrinsic coupling factor for harvesters applications.

coupling factor to 0.33.

4 Extrinsic ME properties

When a device is exposed to an external magnetic field H_0, the internal magnetic field H_3 is reduced by the demagnetization field

$$H_3' = H_0 + H_d = H_0 - N_3 M \tag{13}$$

where H_d is the demagnetizing field, N_3 is the demagnetizing factor in direction 3, and M is the magnetization. The magnetization can be written as follows [32]

$$M = \frac{H_0(\mu_r - 1)}{1 + N_3(\mu_r - 1)} \tag{14}$$

resulting in

$$H_3' = H_0 \frac{\mu_0}{\mu_0 + N_3(\mu - \mu_0)} \tag{15}$$

where H_3' is the magnetic field inside the composite material when the magnetic behavior of the PE phase is assumed to be blended with the surrounding medium (the PM phase is the only phase which has an effect on demagnetization, not the PE). The $'$ symbol is used to differentiate H_3' from H_3, which is the magnetic field inside the composite material when the magnetic behavior of the PE phase is homogenized with the PM phase, as in [21]. We shall see in Section 4.1 and 4.2 that $H_3' = H_3$ for longitudinal magnetization but $H_3' \neq H_3$ for transverse magnetization.

Furthermore, H_0 is the externally applied magnetic field, μ is the magnetic permeability of the material, μ_0 is the magnetic permeability of vacuum, $\mu_r = \mu/\mu_0$ and N_3 is the demagnetizing factor in the 3 direction (the direction in which the magnetic field is applied). N_3 is a function of the geometry of the device.

The demagnetizing factor has values between 0 and 1. When $N_3 = 0$, $H_3' = H_0$ and when $N_3 = 1$, $H_3' = H_0/\mu_r$. Devices with high demagnetizing factor N_3 made with materials having high relative permeability μ_r experience the highest reduction of internal magnetic field H_3'. While intrinsic material performance is independent of geometry, the extrinsic

device performance, i.e., the voltage generated for a given magnetic field, is a function of the dimensions of the device as well as intrinsic performance. The extrinsic performance can be calculated in terms of the intrinsic material performance and the demagnetizing factor for particular device dimensions [33, 34].

The demagnetization factor satisfies the condition $N_1 + N_2 + N_3 = 1$. The simplest case is for an sphere, for which $N_i = 1/3$ and constant in all directions. In the case of an infinite plate, the out of plane demagnetizing factor is 1 and the in-plane demagnetizing factor is 0. For example, for a thin ME laminate in the shape of a large square plate, the TT configuration suffers because $N_3 \to 1$, but the LT and LL configurations have the advantage because $N_3 \to 0$.

The demagnetizing factor for non-infinite plates as a function of position can be calculated using the equations of Joseph and Schlomann [33]. The averaged demagnetization factor can be obtained using the expressions derived by Aharoni [34]. Thus, the dimensions of the ME device can be optimized taking into account the demagnetizing factor N_3. The optimal dimensions would yield $N_3 \to 0$.

For the case of composites with longitudinal magnetization (LT and LL), the thickness has to be considerably smaller than the in-plane dimensions to approach $N \to 0$. For composites with transverse magnetization (TT and TL), measured performance, rather than intrinsic performance, may be significantly reduced due to high demagnetization factor [35].

The demagnetizing factor N_3 is constant inside an ellipsoid but not inside a cuboid [33]. To take into account the variation of the demagnetizing factor at different positions, the constitutive equations have to be solved at every point and integrated trough the volume, drastically increasing the complexity of the analysis. To simplify the analysis, in this work an approximation is used; the demagnetizing factor is averaged through the volume. This allows to us obtain explicit formulas for the ME coefficients.

The averaged demagnetizing factor is calculated using the following formula [34]

$$
\begin{aligned}
\pi N_3 \;=\; & \frac{b^2-c^2}{2bc}\ln\left(\frac{\sqrt{a^2+b^2+c^2}-a}{\sqrt{a^2+b^2+c^2}+a}\right)+\frac{a^2-c^2}{2ac}\ln\left(\frac{\sqrt{a^2+b^2+c^2}-b}{\sqrt{a^2+b^2+c^2}+b}\right) \\
& +\frac{b}{2c}\ln\left(\frac{\sqrt{a^2+b^2}+a}{\sqrt{a^2+b^2}-a}\right)+\frac{a}{2c}\ln\left(\frac{\sqrt{a^2+b^2}+b}{\sqrt{a^2+b^2}-b}\right) \\
& +\frac{c}{2a}\ln\left(\frac{\sqrt{b^2+c^2}-b}{\sqrt{b^2+c^2}+b}\right)+\frac{c}{2b}\ln\left(\frac{\sqrt{a^2+c^2}-a}{\sqrt{a^2+c^2}+a}\right) \\
& +2\arctan\left(\frac{ab}{c\sqrt{a^2+b^2+c^2}}\right)+\frac{a^3+b^3-2c^3}{3abc} \\
& +\frac{a^2+b^2-2c^2}{3abc}\sqrt{a^2+b^2+c^2}+\frac{c}{ab}(\sqrt{a^2+c^2}+\sqrt{b^2+c^2}) \\
& -\frac{(a^2+b^2)^{3/2}+(b^2+c^2)^{3/2}+(c^2+a^2)^{3/2}}{3abc}
\end{aligned}
\tag{16}
$$

where c is the length of the PM phase in the direction of the applied field (direction 3), and a, b, are the dimensions of the PM phase perpendicular to the applied field.

Equation (16) does not apply to a composite with two or more different phases. Fortunately, since the magnetic permeability of the PE phase $\mu^{PE} \approx \mu_0$, it can be blended

with the surrounding medium. Then, the dimensions used in Equation 16 correspond to the dimensions of the PM lamina only. Additionally, the magnetic permeability of the material used in Equation 15 has to be that of the PM phase only. This will be further discussed for each extrinsic property calculated.

4.1 Extrinsic ME voltage coefficient

The extrinsic ME voltage coefficient $\hat{\alpha}$, which depends in the actual geometry of the composite is defined as

$$\hat{\alpha} = \frac{E}{H_0}\Big]_{D=0} \tag{17}$$

The intrinsic ME voltage coefficient for the homogenized composite subject to magnetic field H_3 (see Section 4), is defined [21] as

$$\alpha = \frac{E}{H_3}\Big]_{D=0} \tag{18}$$

At this point is convenient to define the intrinsic ME voltage coefficient for the homogenized composite subject to magnetic field H_3' (which is relevant in the magnetic phase only), as follows

$$\alpha' = \frac{E}{H_3'}\Big]_{D=0} \tag{19}$$

which is similar to α but with the magnetic field applied at the boundaries of the magnetic phase only. There are two different cases. First, when longitudinal magnetization is used, $H_3' = H_3$ and $\alpha' = \alpha$. The second case is when the composite is magnetized in the transverse direction, for which the magnetic field H_3 through the composite is

$$H_3 = \chi H^{PM} + (1-\chi)H^{PE} \tag{20}$$

Thus, α' has to be calculated using (19) for all the composites with transverse magnetization. Finally, the extrinsic voltage coefficient $\hat{\alpha}$ can be obtained as follows

$$\begin{aligned} \frac{\hat{\alpha}}{\alpha'} = \frac{E}{H_0} \times \frac{H_3'}{E}\Big]_{D=0} = \frac{H_3'}{H_0} = \Big]_{D=0} \\ \frac{\hat{\alpha}}{\alpha'} = \frac{\mu_0}{\mu_0 + N_3(\mu' - \mu_0)}\Big]_{D=0} \end{aligned} \tag{21}$$

where $\mu']_{D=0}$ is the magnetic permeability of the PM phase mechanically clamped to the PE phase and with $D = 0$, which can be calculated as

$$\mu']_{D=0} = \frac{B_3'}{H_3'}\Big]_{D=0} = \frac{B^{PM}}{H^{PM}}\Big]_{D=0} \tag{22}$$

where B_3' is the magnetic flux in the magnetic phase only.

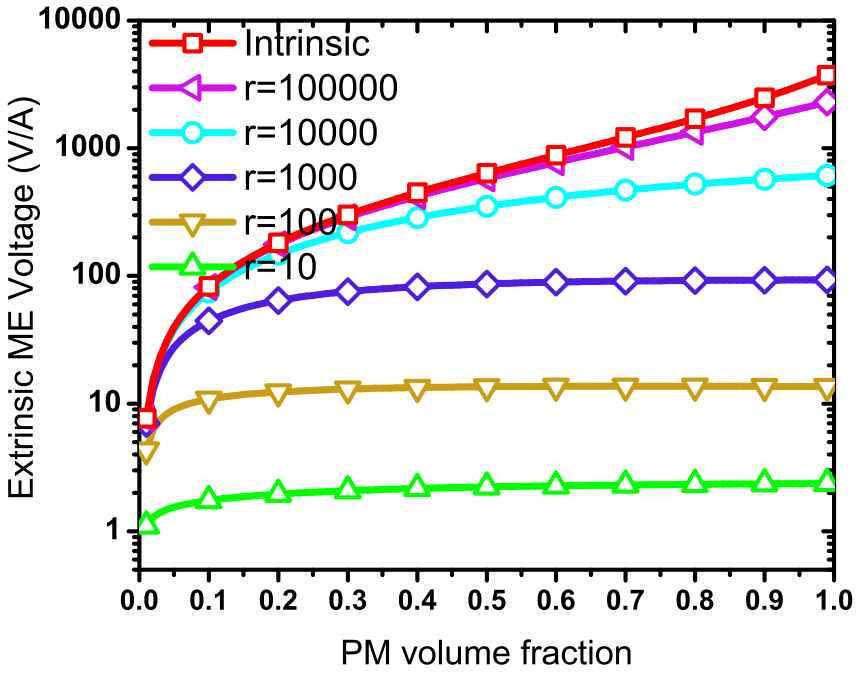

Figure 11: Extrinsic ME voltage coefficient for Metglas/PZT-2 in LL configuration for aspect ratios of 10, 100, 10000, and $r \to \infty$ (intrinsic value).

Analytical expressions for $\mu']_{D=0}$ in all four configurations are developed in this work by solving the constitutive equations subjected to appropriate boundary conditions for each configuration. For the LL configuration the following expression is obtained

$$\mu_{LL}]_{D=0} = \frac{\epsilon_{33}^{PE}(A_1+B_1+C_1+D_1)+\chi(E_1+F_1+G_1)}{\epsilon_{33}^{PE}(H_1+I_1)+\chi(J_1+K_1)} \tag{23}$$

$$\begin{aligned}
A_1 &= (q_{33}^{PM})^2(\chi-1)(S_{11}^{PM}(\chi-1)-S_{11}^{PE}\chi)-2q_{31}^{PM}q_{33}^{PM}(\chi-1)(S_{23}^{PM}(\chi-1)-S_{23}^{PE}\chi)\\
B_1 &= (q_{31}^{PM})^2(\chi-1)(S_{33}^{PM}(\chi-1)-S_{33}^{PE}\chi)+\mu_{33}^{PM}((S_{23}^{PM})^2-S_{11}^{PM}S_{33}^{PM}\\
C_1 &= -(2S_{23}^{PM}(S_{23}^{PM}-S_{23}^{PE})+S_{11}^{PM}(S_{33}^{PE}-2S_{33}^{PM})+S_{11}^{PE}S_{33}^{PM})\chi\\
D_1 &= ((S_{23}^{PE}-S_{23}^{PM})^2-(S_{11}^{PE}-S_{11}^{PM})(S_{33}^{PE}-S_{33}^{PM}))\chi^2))\\
E_1 &= (d_{33}^{PE})^2((q_{31}^{PM})^2(\chi-1)+\mu_{33}^{PM}(S_{11}^{PM}+S_{11}^{PE}\chi-S_{11}^{PM}\chi))\\
F_1 &= -2d_{31}^{PE}d_{33}^{PE}(q_{31}^{PM}q_{33}^{PM}(\chi-1)+\mu_{33}^{PM}(S_{23}^{PM}+S_{23}^{PE}\chi-S_{23}^{PM}\chi))\\
G_1 &= (d_{31}^{PE})^2((q_{33}^{PM})^2(\chi-1)+\mu_{33}^{PM}(S_{33}^{PM}+S_{33}^{PE}\chi-S_{33}^{PM}\chi))\\
H_1 &= (S_{23}^{PM})^2-S_{11}^{PM}S_{33}^{PM}-(S_{33}^{PE}S_{11}^{PM}+2S_{23}^{PM}(-S_{23}^{PE}+S_{23}^{PM})+(S_{11}^{PE}-2S_{11}^{PM})S_{33}^{PM})\chi\\
I_1 &= ((S_{23}^{PE}-S_{23}^{PM})^2-(S_{11}^{PE}-S_{11}^{PM})(S_{33}^{PE}-S_{33}^{PM}))\chi^2\\
J_1 &= 2d_{31}^{PE}d_{33}^{PE}(S_{23}^{PM}(\chi-1)-S_{23}^{PE}\chi)+(d_{33}^{PE})^2(S_{11}^{PM}+S_{11}^{PE}\chi-S_{11}^{PM}\chi)\\
K_1 &= (d_{31}^{PE})^2(S_{33}^{PM}+S_{33}^{PE}\chi-S_{33}^{PM}\chi)
\end{aligned}$$

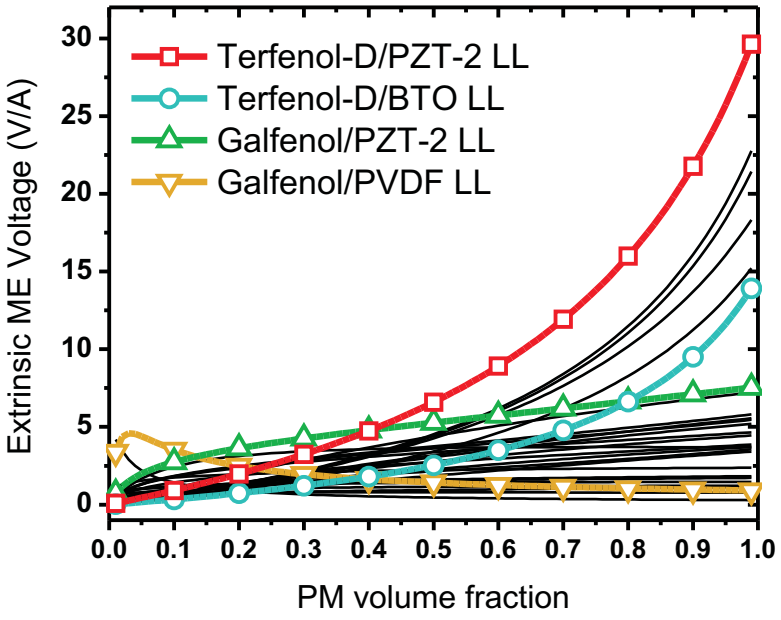

Figure 12: Extrinsic ME voltage coefficient for all the material combinations for an aspect ratio of $r = 10$.

Equation (23) and a similar expression for the LT configuration (not shown in this paper) can be found in the Website [31].

Values of extrinsic ME voltage coefficient are calculated for Metglas/PZT-2 composite in LL configuration and the results are shown in Figure 11. These results were calculated using a composite with equal length and width (square in-plane) and various thicknesses. The aspect ratio r is defined as follows

$$r = \frac{c}{t} = \frac{a}{t} \tag{24}$$

where a is the width of the composite, c is the length of the composite (in the direction of the applied magnetic field) and t is the total thickness of the composite. Therefore, the thickness b of the PM phase is obtained in terms of the PM volume fraction as $b = \chi\, t$. It can be seen in Figure 11 that when the aspect ratio is reduced, the extrinsic ME voltage decreases.

Intrinsic properties are obtained when $r \to \infty$ because the demagnetizing factor approaches zero ($N_3 \to 0$). Very high values for the aspect ratio are required to preserve the intrinsic properties in the case of Metglas. This is due to its high magnetic permeability, making it very sensitive to demagnetizing effects. For example, if the aspect ratio is $r = 10^4$ for Metglas/PZT-2 LL, the extrinsic ME voltage is $\hat{\alpha} = 581 V A^{-1}$, which is considerably smaller than the intrinsic value of $\alpha = 2705 V A^{-1}$, where both values are calculated using $\chi = 92\%$ to retain 70 % of the maximum intrinsic ME coupling factor. In practice, aspect

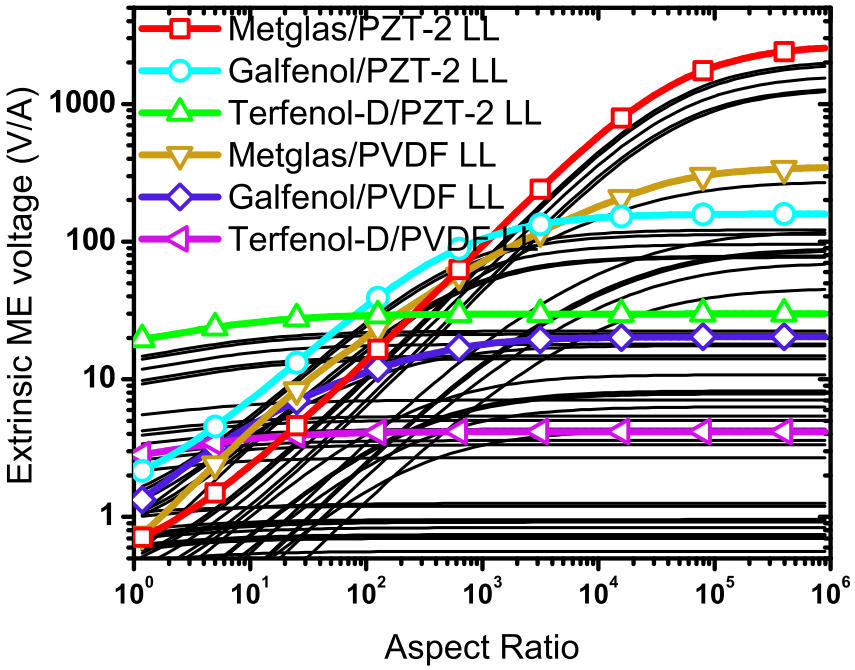

Figure 13: Extrinsic ME voltage coefficient for all the ME composite proposed as a function of the device aspect ratio. The optimum PM volume fraction for each material combination can be seen in Figure 14.

ratios of $r = 10$ are preferred to facilitate the fabrication of the device. In such case, the extrinsic ME voltage coefficient decreases to $\hat{\alpha} = 2.4VA^{-1}$, which is 10^3 times smaller than the intrinsic value.

Since ME voltage decreases so drastically for Metglas/PZT-2 for small aspect ratios, other materials with smaller magnetic permeability are investigated to see if they can sustain higher extrinsic ME voltage. Results for all material combinations in LL configuration are shown in Figure 12 for aspect ratio $r = 10$. It can be seen that composites with Terfenol-D have the highest extrinsic ME voltage due to their smaller magnetic permeability. With regards to the PE phase, PZT-2 allows for the highest extrinsic ME voltage. Terfenol-D/PZT-2 has the highest extrinsic ME voltage $\hat{\alpha} = 26VA^{-1}$ for a PM volume fraction of $\chi = 95\%$. Using Galfenol instead of Terfenol-D results in a lower $\hat{\alpha}$ due to the higher magnetic permeability of Galfenol.

The effect of the aspect ratio can be seen in Figure 13. The demagnetizing effect is stronger for materials with higher magnetic permeability, resulting in higher decrease of the extrinsic ME voltage. It can be seen in Figure 13 that Metglas/PZT-2 has the highest $\hat{\alpha}$ for aspect ratios higher than $r > 1200$. For small aspect ratios ($r < 90$), Terfenol-D/PZT-2 shows the highest extrinsic ME voltage, and between these aspect ratios, Galfenol/PZT-2 has the highest $\hat{\alpha}$.

The PM volume fraction used in Figure 13 is the optimum for each composite and aspect

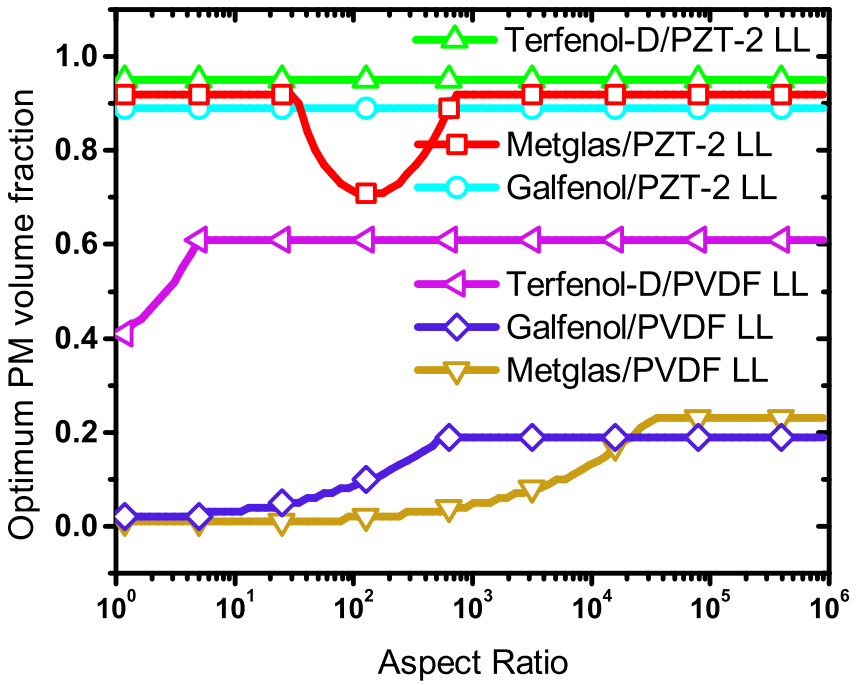

Figure 14: Optimum PM volume fraction (dimensionless) to maximize $\hat{\alpha}$, of Terfenol-D/PZT-2, Galfenol/PZT-2, Metglas/PZT-2, and Metglas/PVDF in LL configuration as a function of the device aspect ratio.

ratio, which in some cases has to be reduced from the optimum of $\chi = 1$ to a vales retaining 70 % of the intrinsic ME coupling factor. In the case of Terfenol-D/PZT-2 and Galfenol/PZT-2 in the LL configuration, the optimum PM volume fraction is $\chi = 1$, so they are reduced to 95 and 89 %, respectively.

For Metglas/PZT-2 and Metglas/PVDF in LL configuration, the optimum PM volume fraction changes with aspect ratio, as it can be seen in Figure 14. In the case of Metglas/PVDF for aspect ratios larger than 35000 the optimum PM volume fraction is given by the 70% retention criterion. When $r < 35000$ is used, the optimum PM volume fraction decreases. The intrinsic ME voltage coefficient does not change when different aspect ratios are used but the demagnetizing factor does. For smaller PM volume fraction, the demagnetizing factor decreases because the thickness of the PM lamina used in (16) decreases. In some cases, like for Metglas/PVDF, the decrease in the demagnetizing factor (due to smaller optimum PM volume fraction required to stretch the PVDF) has a positive effect that more than compensates for the decrease in the intrinsic ME voltage resulting from using PVDF. This effect can be easily noticed for PVDF because PVDF is a soft PE material, not needing a thick PM lamina with high stiffness to strain it. A similar effect can be seen for Metglas/PZT-2 and for all the composites using Metglas.

In Figure 14, demagnetization is negligible for aspect ratio $r = 10^6$ and a thick PM layer ($\chi = 92\%$) is needed for optimum performance. As r decreases from right to left,

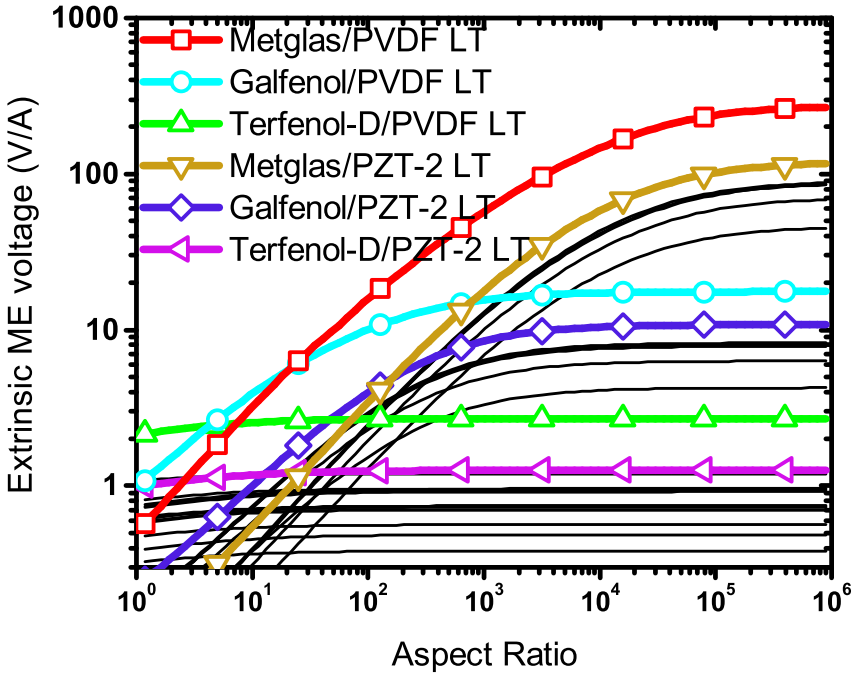

Figure 15: Extrinsic ME voltage coefficient all the ME composites in LT configuration as a function of the device aspect ratio. The optimum PM volume fraction for each configuration can be seen in Figure 16.

demagnetization grows. For Metglas/PZT-2 LL and $30 < r < 500$, reducing χ reduces demagnetization more that enough to compensate for the reduction of magnetostriction, an thus ME voltage α, due to a lower χ. Therefore, the optimum PM volume fraction drops below 92%. However, for $r < 30$, the effect of χ on magnetostriction overcomes the reduction of demagnetization, so the optimum goes back to $\chi = 92\%$. This behavior can be seen also for Galfenol/PVDF LL and Terfenol-D/PVDF LL with $r < 700$ and $r < 4$, respectively.

The LL configuration yields maximum extrinsic ME voltage. However, LL configuration requires an insulating layer to prevent current leakage, thus fabrication is more complex. For this reason the LT configuration (most commonly used in the literature) is studied independently from the LL configuration. The predictions are shown in Figure 15.

LT Metglas/PVDF has the highest intrinsic voltage, as it is discussed in Section 3.2.2. Metglas/PVDF is the best option when aspect ratios higher than 250 are used. When aspect ratios from 4 to 250 are used, Galfenol/PVDF has the highest extrinsic ME voltage, and for aspect ratios smaller than 4, Terfenol-D/PVDF is the best candidate, because it has high compliance, requiring less PM thickness to stretch it, thus resulting in a thicker PE, which effectively increases the electric field. Note that since the PM volume fraction for the composites with PVDF are small, resulting in a thin PM layer, the demagnetizing effect has a smaller impact than for other composites.

As it can be seen in Figure 16, the optimum PM volume fraction for LT Metglas/PVDF

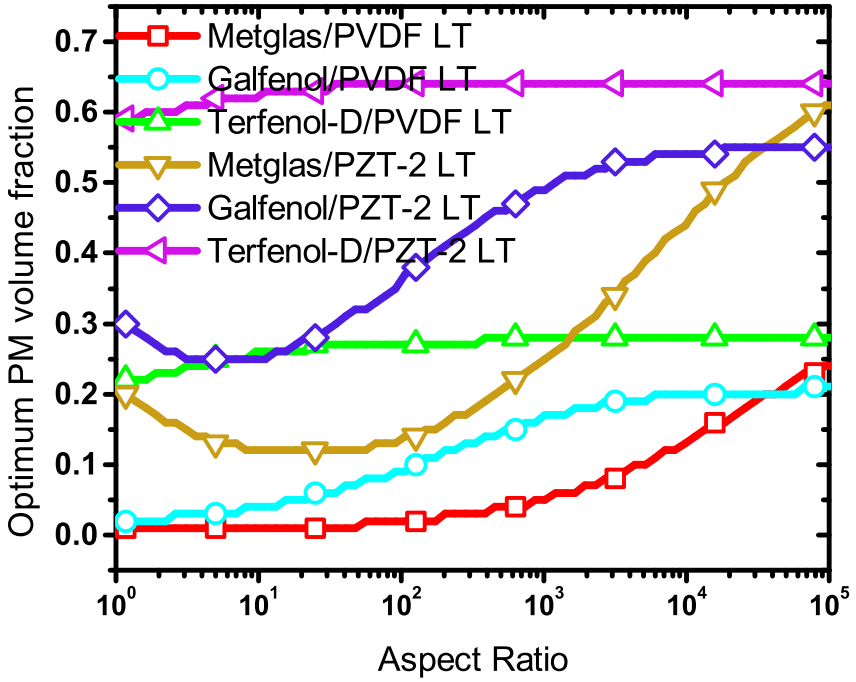

Figure 16: Optimum PM volume fraction (dimensionless) of Terfenol-D/PVDF, Galfenol/PVDF, Metglas/PVDF, Terfenol-D/PZT-2, Galfenol/PZT-2, and Metglas/PZT-2 in LT configuration as a function of the device aspect ratio.

composite increases when aspect ratio increases. The optimum PM volume fraction for the intrinsic case (represented in the plot by $r = 10^6$) is 23 %. When aspect ratios smaller that 300 are used, the optimum PM volume fraction is 1%. This is due to the fact that smaller PM volume fraction results in smaller demagnetizing factor because the thickness of the PM phase is smaller. Furthermore, the PM phase does not need to have high stiffness because PVDF has a high compliance.

For LT Metglas/PVDF composite with $\chi \to 1\%$, the intrinsic ME coupling factor plateaus at 75% of the highest ME coupling factor achievable. Thus, it satisfies the 70% retention criterion even at $\chi \to 1\%$. If a PE phase with a lower compliance is used, such as in Metglas/PZT-2 composite, the optimum PM volume fraction does not decrease as much as for Metglas/PVDF because a thicker PM phase is required to drive the relatively stiff PZT-2.

A similar effect to the one shown by Metglas/PVDF can be seen with Galfenol/PVDF and Terfenol-D/PVDF, but in these composites the decrease in optimum PM volume fraction with decreasing aspect ratio is less severe than for Metgals/PVDF due to smaller magnetic permeability of Galfenol and Terfenol-D. An additional advantage of using PVDF instead of PZT materials is that PVDF is lead-free.

4.2 Extrinsic ME charge coefficient

Similarly to Section 4.1, the extrinsic ME charge coefficient $\hat{\beta}$ is defined as

$$\hat{\beta} = \frac{D}{H_0}\Big]_{E=0} \tag{25}$$

The intrinsic ME charge coefficient for the homogenized composite subject to magnetic field H_3 (see Section 4), is defined [21] as

$$\beta = \frac{D}{H_3}\Big]_{E=0} \tag{26}$$

At this point is convenient to define the intrinsic ME charge coefficient for the homogenized composite subject to magnetic field H_3' (which is relevant in the magnetic phase only), as follows

$$\beta' = \frac{D}{H_3'}\Big]_{E=0} \tag{27}$$

which results in

$$\begin{aligned} \frac{\hat{\beta}}{\beta'} = \frac{D}{H_0} \times \frac{H_3'}{D}\Big]_{E=0} = \frac{H_3'}{H_0}\Big]_{E=0} = \\ \frac{\hat{\beta}}{\beta'} = \frac{\mu_0}{\mu_0 + N_3(\mu' - \mu_0)}\Big]_{E=0} \end{aligned} \tag{28}$$

where β' and μ' are defined in the same way as in Section 4.1. In the case of longitudinal magnetization $\beta = \beta'$, but for transverse magnetization β' it has to be calculated using appropriate boundary conditions.

Also note that in (28), the magnetic permeability μ' is the magnetic permeability of the PM phase when mechanically bonded to the PE phase, for a constant electric field $E = 0$, i.e.,

$$\mu' = \frac{B_3'}{H_3'}\Big]_{E=0} = \frac{B^{PM}}{H^{PM}}\Big]_{E=0} \tag{29}$$

which must be calculated using the corresponding boundary conditions. The analytical expression is provided in the Website [31].

Predicted extrinsic ME charge coefficients for composites with aspect ratio $r = 10$ are reported in Figure 17. Terfenol-D/PZT-5H in LT configuration has the best performance ($\hat{\beta} = 77 \times 10^{-9} C\, A^{-1} m^{-1}$ and $\kappa = 0.08$ for $\chi = 95\%$). This is due to the smaller demagnetizing effect in a material, such as Terfenol, with relatively small magnetic permeability. In the LL configuration, the optimum extrinsic ME charge coefficient $\hat{\beta} = 41 \times 10^{-9} C\, A^{-1} m^{-1}$

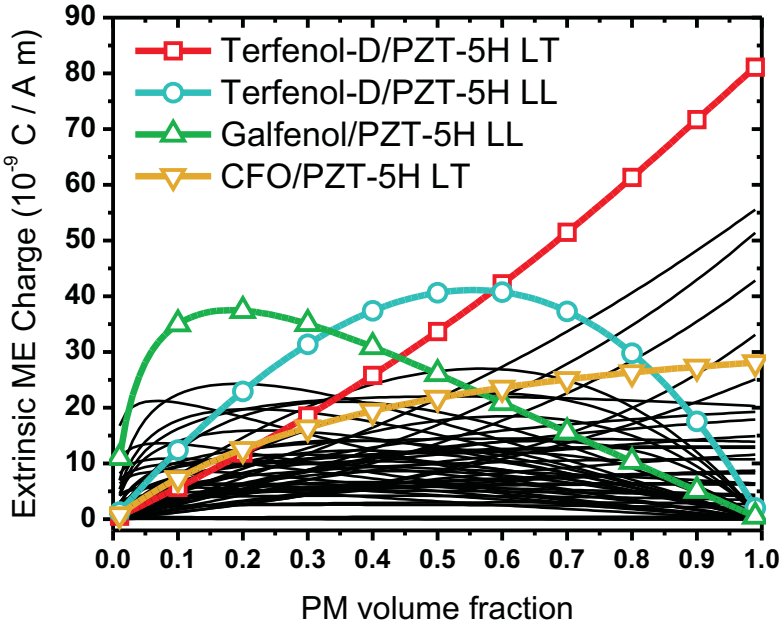

Figure 17: Extrinsic ME charge coefficient for all material combinations and aspect ratio $r = 10$.

is good as well, with the advantage of occurring at $\chi = 55\%$, which has a $\kappa = 0.30$. Even Galfenol, which has higher magnetic permeability than Terfenol, shows a high ME extrinsic charge coefficient of $\hat{\beta} = 38 \times 10^{-9} C\, A^{-1} m^{-1}$, due to the higher intrinsic ME charge coefficient of Galfenol/PZT-5H in LL configuration. The later is just one example where *intrinsic* performance is useful to explain an *extrinsic* feature of a ME composite.

To evaluate the ME charge performance of the 28 ME composites studied in this work, the extrinsic ME charge coefficient as a function of the aspect ratio is calculated and reported in Figure 18. When smaller aspect ratios are used, the demagnetizing effect is stronger for materials with high magnetic permeability, resulting in higher extrinsic ME charge coefficient for materials with smaller magnetic permeability. For aspect ratios $r > 16000$, Metglas/PZT-5H in the LT configuration ($\chi = 95\%$) holds the highest ME charge coefficient. For aspect ratios $126 < r < 16000$, Metglas/PZT-5H in the LL configuration ($\chi = 10\%$ for $r = 126$ and $\chi = 41\%$ for $r = 16000$) shows the highest $\hat{\beta}$. For aspect ratios $37 < r < 126$, Galfenol/PZT-5H in the LL configuration ($\chi = 31\%$) shows the highest $\hat{\beta}$. For aspect ratios $r < 37$, Terfenol-D/PZT-5H in the LT configuration ($\chi = 95\%$) shows the highest $\hat{\beta}$.

The optimum PM volume fraction for each configuration discussed in this Section varies similarly to Figure 14 but it is not shown for sake of space. Actual values can be calculated using the formulas provided Website [31].

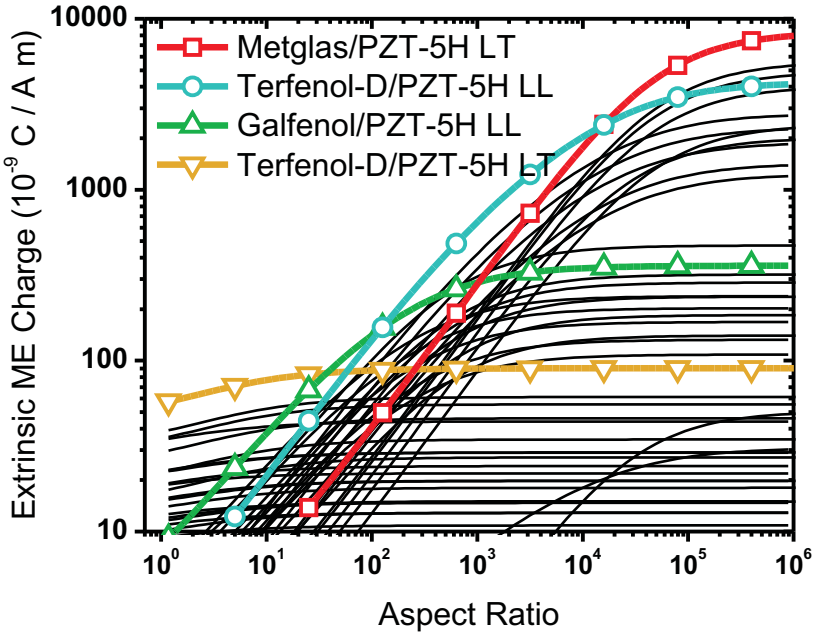

Figure 18: Extrinsic ME charge coefficient for all material combinations as a function of aspect ratio. Optimum PM volume fraction is used in LL configuration. 70% retention volume fraction is used for LT configuration.

4.3 Extrinsic ME coupling factor

The extrinsic ME coupling factor is defined similarly to the intrinsic ME coupling factor in [21], but using the externally applied, specific magnetic work. The later takes into account both the intrinsic work and the work in the surrounding medium (vacuum or air). Therefore,

$$\hat{\kappa}^2 = \frac{W_E^G}{\hat{W}_M^A} \tag{30}$$

were $\hat{W}_M^A$ is the extrinsic magnetic work applied (specific magnetic work externally applied), when the electric field in the composite is constant. The extrinsic magnetic work applied can be obtained as follows

$$\hat{W}_M^A = \frac{B_0 \times H_0}{2}\Big]_{E=0} = \frac{\mu_{ext}(H_0)^2}{2}\Big]_{E=0} \tag{31}$$

were H_0 is the externally applied magnetic field, B_0 is the externally applied magnetic flux, and μ_{ext} is the magnetic permeability of the medium (vacuum, or air) with the composite structure inside. When the magnetic field is applied far enough (at infinity), the value of μ_{ext} approaches the magnetic permeability of vacuum μ_0.

Because the average demagnetizing factor formula (16) only applies to a single phase lamina, in this work the PE phase is included in the surrounding medium and κ' is defined

as

$$(\kappa')^2 = \frac{W_E^G}{W_M'^A} \tag{32}$$

where the extrinsic work applied in terms of magnetic field H_3' in the PM phase is

$$W_M'^A = \frac{B_3' \times H_3'}{2}\Big]_{E=0} = \frac{B^{PM} \times H^{PM}}{2}\Big]_{E=0} = \frac{\mu'(H_3')^2}{2}\Big]_{E=0} \tag{33}$$

and κ' has to be calculated for all four configurations. It can be shown that:

$$(\kappa_{ij}')^2 = \frac{(\beta_{ij}')^2}{\epsilon_{jj}^H \times \mu_{ii}'^E} \tag{34}$$

were ϵ^H is the dielectric constant of the composite at constant magnetic field, calculated in [21]. Next, the extrinsic ME coupling factor can be obtained as follows

$$\left(\frac{\hat{\kappa}}{\kappa'}\right)^2 = \frac{W_E^G}{\hat{W}_M^A} \times \frac{W_M'^A}{W_E^G} = \frac{W_M'^A}{\hat{W}_M^A} = \frac{H_3'}{H_0} \times \frac{B_3'}{B_0}\Big]_{E=0} = \left(\frac{H_3'}{H_0}\right)^2 \times \frac{\mu'}{\mu_0}\Big]_{E=0}$$
$$\left(\frac{\hat{\kappa}}{\kappa'}\right)^2 = \frac{\mu'\mu_0}{(\mu_0 + N_3(\mu' - \mu_0))^2}\Big]_{E=0} \tag{35}$$

Note that μ' is the magnetic permeability of the PM phase, bonded to the PE phase, when the electric field is constant, which has to be calculated.

For aspect ratios $r \to \infty$ the demagnetizing factor $N_3 \to 0$ reducing (35) to

$$\hat{\kappa} = \kappa' \sqrt{\frac{\mu'}{\mu_0}\Big]_{E=0}} \tag{36}$$

This equation implies that $\hat{\kappa} > \kappa'$ because $\mu' > \mu_0$ when a PM material of any kind is present in the medium (air or vacuum). Values of $\hat{\kappa}$ could be higher than unity because (30) is a ratio of specific work over different volumes, with W_E^G measured over the volume of the device and $\hat{W}_M^A$ over the volume where the external magnetic field is applied.

Maximum values of extrinsic ME coupling coefficient (obtained at optimum PM volume fraction for all materials) are shown in Figure 19. It can be seen that Metglas/PZT-5H in LL configuration has the highest ME coupling coefficient for aspect ratios higher than 350. This is due to the fact that Metglas and PZT-5H have the maximum PM and PE coupling factors, respectively. For aspect ratios between 27 and 350 Galfenol/PZT-5H in the LL configuration has the highest extrinsic ME coupling coefficient. As previously discussed, demagnetization is smaller on Galfenol than on Metglas. Finally, for aspect ratios smaller than 27, Terfenol-D/PZT-5H LL has the highest $\hat{\kappa}$.

5 Conclusions

The effects of demagnetization are drastic, not only in magnitude but also drastically changing material selection and volume fraction, both as function of the device's geometrical aspect

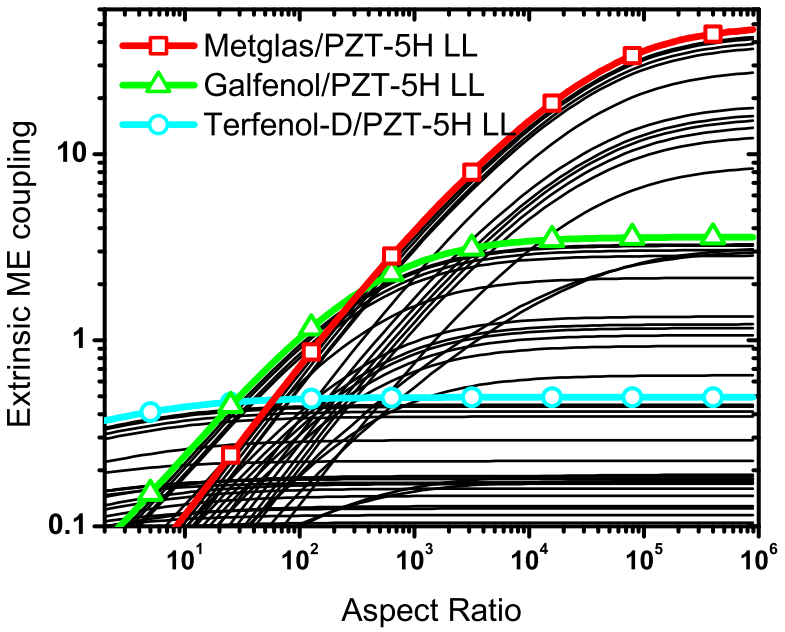

Figure 19: Optimum extrinsic ME coupling factor (dimensionless) for all material combinations as a function of aspect ratio.

ratio. PM materials with high magnetic permeability are very sensitive to demagnetizing effects and loose their comparative advantage even if they also posses high intrinsic coupling. There are two ways to minimize demagnetization: use a PM with low permeability μ or a PE with high compliance S. A composite with low PM permeability μ is better because the usable magnetic field H_3 in (15) is inversely proportional to μ, so less μ means the performance is less affected by demagnetization. A composite with high PE compliance (e.g., PVDF) is best in LT and LL configurations because less PM is needed, and since only the PM is affected by demagnetization, the extrinsic performance is less affected.

The material combinations identified as having best intrinsic performance are replaced by different material combinations when extrinsic properties are calculated. Furthermore, the best material selection, optimum volume fraction, and even optimal configuration vary with the aspect ratio, thus requiring to include device geometry in the design process. The LL configuration yields maximum *extrinsic* ME voltage. For an aspect ratio of 10, ME devices based on Terfenol-D are predicted to have the highest extrinsic voltage coefficient due to its relatively small magnetic permeability $\mu_{33}/\mu_0 = 3$ (Table 2). In some cases, like for Metglas/PVDF, the decrease in the demagnetizing factor (due to smaller optimum PM volume fraction required to stretch the compliant PVDF) has a positive effect that more than compensates for the decrease in the intrinsic ME voltage resulting from using PVDF. However, different PM phases are required to achieve optimum performance at different values of aspect ratio.

The highest *extrinsic* α and κ are predicted when the ME composite is polarized and magnetized in the longitudinal direction, justifying the more complicated fabrication required

by longitudinal polarization, which requires an insulator to prevent charge leakage from the PE phase through the PM phase. Longitudinal magnetization yields higher *extrinsic* open circuit sensitivity due to the higher strain produced.

6 Acknowledgment

The authors wish to thank the Energy Materials Science and Engineering Program (EMSE) at West Virginia University for financial and infrastructure support.

References

[1] S. Dong, J. Zhai, F. Bai, J.-F. Li, and D. Viehland, "Push-pull mode magnetostrictive/piezoelectric laminate composite with an enhanced magnetoelectric voltage coefficient," *Applied Physics Letters*, vol. 87, no. 6, p. 062502, 2005.

[2] J. Huang, R. O'Handley, and D. Bono, "New, high-sensitivity, hybrid magnetostrictive/electroactive magnetic field sensors," *Proceedings of SPIE - The International Society for Optical Engineering*, vol. 5050, pp. 229–237, 2003.

[3] S. Roundy and Y. Zhang, "Toward self-tuning adaptive vibration based microgenerators," *Proceedings of SPIE - The International Society for Optical Engineering*, vol. 5649, no. PART 1, pp. 373–384, 2005.

[4] P. Li, Y. Wen, and L. Bian, "Enhanced magnetoelectric effects in composite of piezoelectric ceramics, rare-earth iron alloys, and ultrasonic horn," *Applied Physics Letters*, vol. 90, no. 2, p. 022503, 2007.

[5] S. Dong, J. Zhai, J. F. Li, D. Viehland, and S. Priya, "Multimodal system for harvesting magnetic and mechanical energy," *Applied Physics Letters*, vol. 93, no. 10, p. 103511, 2008.

[6] I. Sari, T. Balkan, and H. Kulah, "An electromagnetic micro power generator for wideband environmental vibrations," *Sensors and Actuators, A: Physical*, vol. 145-146, no. 1-2, pp. 405–413, 2008.

[7] X. Dai, Y. Wen, P. Li, J. Yang, and G. Zhang, "Modeling, characterization and fabrication of vibration energy harvester using Terfenol-D/PZT/Terfenol-D composite transducer," *Sensors and Actuators A: Physical*, vol. 156, no. 2, pp. 350 – 358, 2009.

[8] S. D. Moss, J. E. McLeod, I. G. Powlesland, and S. C. Galea, "A bi-axial magnetoelectric vibration energy harvester," *Sensors and Actuators A: Physical*, vol. 175, no. 0, pp. 165 – 168, 2012.

[9] Z. Shi, C. Wang, X. Liu, and C. Nan, "A four-state memory cell based on magnetoelectric composite," *Chinese Science Bulletin*, vol. 53, no. 14, pp. 2135–2138, 2008.

[10] G. T. Rado and V. J. Folen, "Observation of the magnetically induced magnetoelectric effect and evidence for antiferromagnetic domains," *Physical review letters*, vol. 7, pp. 310–311, 1961.

[11] G. T. Rado, J. M. Ferrari, and W. G. Maisch, "Magnetoelectric susceptibility and magnetic symmetry of magnetoelectrically annealed $TbPO_4$," *Physical review B*, vol. 29, pp. 4041–4048, 1984.

[12] J. Boomgaard, D. R. Terrell, R. A. J. Born, and H. F. J. I. Giller, "An in situ grown eutectic magnetoelectric composite material," *Journal of Materials Science*, vol. 9, pp. 1705–1709, 1974.

[13] J. Ryu, S. Priya, A. V. Carazo, K. Uchino, and H.-E. Kim, "Effect of the magnetostrictive layer on magnetoelectric properties in lead zirconate titanate/terfenol- D laminate composites," *Journal of the American Ceramic Society*, vol. 84, no. 12, pp. 2905–2908, 2001.

[14] S. Priya, J. Ryu, C.-S. Park, J. Oliver, J.-J. Choi, and D.-S. Park, "Piezoelectric and magnetoelectric thick films for fabricating power sources in wireless sensor nodes," *Sensors*, vol. 9, no. 8, pp. 6362–6384, 2009.

[15] R. Kambale, D.-Y. Jeong, and J. Ryu, "Current status of magnetoelectric composite thin/thick films," *Advances in Condensed Matter Physics*, vol. 2012, p. 824643, 2012.

[16] T. I. Muchenik and E. J. Barbero, "Magnetoelectric composites," in *Multifunctional Composites* (E. J. Barbero, ed.), Charleston, SC: CreateSpace, 2015.

[17] G. Harshe, J. Dougherty, and R. Newnham, "Theoretical modelling of multilayer magnetoelectric composites," *International journal of applied electromagnetics in materials*, vol. 4, no. 2, pp. 145–159, 1993.

[18] C.-W. Nan, "Magnetoelectric effect in composites of piezoelectric and piezomagnetic phases," *Physical Review B*, vol. 50, pp. 6082–6088, 1994.

[19] I. Osaretin and R. Rojas, "Theoretical model for the magnetoelectric effect in magnetostrictive/ piezoelectric composites," *Physical Review B - Condensed Matter and Materials Physics*, vol. 82, no. 17, p. 174415, 2010.

[20] M. Bichurin and V. Petrov, "Modeling of magnetoelectric interaction in magnetostrictive-piezoelectric composites," *Advances in Condensed Matter Physics*, vol. 2012, p. 798310, 2012.

[21] T. I. Muchenik and E. J. Barbero, "Charge, voltage, and work-conversion formulas for magnetoelectric laminated composites," *Smart Mater. Struct.*, vol. 24, no. 025039, p. 025039, 2015.

[22] S. Dong, J.-F. Li, and D. Viehland, "Magnetoelectric coupling, efficiency, and voltage gain effect in piezoelectric-piezomagnetic laminate composites," *Journal of Materials Science*, vol. 41, no. 1, pp. 97–106, 2006.

[23] K. Sun and Y. Kim, "Design of magnetoelectric multiferroic heterostructures by topology optimization," *Journal of Physics D: Applied Physics*, vol. 44, no. 18, p. 185003, 2011.

[24] D. Berlincourt and H. H. A. Krueger, "Properties of morgan electro ceramic ceramics," tech. rep., Morgan Electro Ceramics.

[25] C. Sherman and J. Butler, *Transducers and Arrays for Underwater Sound*. The Underwater Acoustics Series, Springer, 2007.

[26] D. M. Esterly, *Manufacturing of Poly(vinylidene fluoride) and Evaluation of its Mechanical Properties*. PhD thesis, Virginia Polytechnic Institute and State University, 2002.

[27] G. Srinivasan, E. T. Rasmussen, and R. Hayes, "Magnetoelectric effects in ferrite-lead zirconate titanate layered composites: The influence of zinc substitution in ferrites," *Phys. Rev. B*, vol. 67, p. 014418, Jan 2003.

[28] E. Barbero, *Finite Element Analysis of Composite Materials Using Abaqus*. Composite Materials: Analysis and Design Series, Boca Raton, FL: Taylor and Francis, 2013.

[29] C.-M. Chang and G. Carman, "Modeling shear lag and demagnetization effects in magneto-electric laminate composites," *Physical Review B - Condensed Matter and Materials Physics*, vol. 76, no. 13, p. 134116, 2007.

[30] S. Dong, J. Zhai, J. Li, and D. Viehland, "Near-ideal magnetoelectricity in high-permeability magnetostrictive/ piezofiber laminates with a (2-1) connectivity," *Applied Physics Letters*, vol. 89, no. 25, p. 252904, 2006.

[31] Web resource, 2014. http://barbero.cadec-online.com/papers/source/ME/laminate/.

[32] B. D. Cullity and C. D. Graham, *Experimental Methods*, pp. 23–86. John Wiley & Sons, Inc., 2008.

[33] R. Joseph and E. Schlomann, "Demagnetizing field in nonellipsoidal bodies," *Journal of Applied Physics*, vol. 36, no. 5, pp. 1579–1593, 1965.

[34] A. Aharoni, "Demagnetizing factors for rectangular ferromagnetic prisms," *Journal of Applied Physics*, vol. 83, no. 6, pp. 3432–3434, 1998.

[35] E. Quandt, S. Stein, and M. Wuttig, "Magnetic vector field sensor using magnetoelectric thin-film composites," *IEEE Transactions on Magnetics*, vol. 41, no. 10, pp. 3667–3669, 2005.